Chapter 6. Magnets

Frederick Mills and Jean-François Ostiguy

6.1. Introduction

To accelerate and deliver 1 MW of beam power at 16 GeV while keeping space charge induced tune shift and tune spread at acceptable levels, the Fermilab Proton driver uses rapid cycling magnets with unusually large apertures. Space charge mitigation is accomplished by spreading out the charge both transversely and longitudinally. The aperture size, which is a principal cost driver, is determined not only by the need to accommodate large transverse beam sizes to reduce the tune shift, but also to keep losses at a level compatible with safety requirements. The chosen magnet apertures should be adequate to keep the worst case injection losses below 10 %, that is 2.5 kW out of the 25 kW total beam power at injection.

Aside from the fact that large stored energy and rapid cycling lead to substantial power supply costs, many aspects of the proton driver magnets are challenging, including high voltage insulation, eddy-current power loss minimization and eddy current induced field errors compensation.

It is worth mentioning that because the space charge tune shift scales as $\beta^{-1}\gamma^{-2}$, increasing the injection energy – currently set to 400 MeV by the existing FNAL linac – would significantly reduce the cost of magnet and related subsystems and possibly reduce technical risks as well, at the expense of more linac rf. A detailed discussion of the trade-offs can be found in Appendix B.

The presence of large energy dependent space charge tune shift and tune spread dictates the need for tight tracking between the quadrupole and bending dipole magnets during the entire acceleration cycle. Quadrupole tracking error is effectively equivalent to momentum offset error and results in a tune shift of magnitude

$$\Delta\nu = \xi_{\text{uncorrected}} \left[\frac{\Delta G}{G} - \frac{\Delta B}{B} \right] \tag{6.1}$$

$$= \xi_{\text{uncorrected}} \left[\frac{\Delta(G/B)}{(G/B)} \right] \tag{6.2}$$

where $\frac{\Delta G}{G}$ and $\frac{\Delta B}{B}$ are respectively the relative gradient and main dipole field errors. Note that the tune variation is proportional to $\xi_{\text{uncorrected}}$, the *uncorrected* chromaticity because, in the context of a quadrupole tracking error, there is no closed orbit error and the chromaticity correction sextupoles have no effect.

The magnitude of the tolerable tune shift is arguable. Although tracking is expected to become less critical as energy increases, in the context of this report, we *conservatively* de-

mand that

$$\Delta\nu < 0.01 \tag{6.3}$$

during the *entire* cycle. This requirement is based on the ISIS experience, where the ability to control the tune at that level was shown to be necessary in order to avoid specific resonances at extraction. While it is possible that the upper limit for the tolerable tracking error induced tune shift may turn out to be be larger, this report errs on the conservative side, in absence of the availability of detailed simulations.

In some machines like the Fermilab Booster, good tracking is naturally achieved by employing combined function magnets operating well below 1 T, far away from saturation. In contrast, the Proton Driver lattice is based on separate function magnets with main bending dipoles operating at an aggressive 1.5 T peak field. This field was chosen to simultaneously make the circumference ratio between the Main Injector and the Proton Driver a simple rational fraction (for synchronous beam transfers) and minimize the space charge tune shift, which is proportional to the machine circumference. While the magnet transfer function starts deviating from linearity above 1 T, this can be compensated for by a combination of careful quadrupole and dipole saturation matching supplemented by an active quadrupole correction system. Admittedly, 1.5 T is not a very precisely defined limit; however, it is fair to say that above 1.5 T, the nonlinearity becomes too substantial for active correction to be practical.

6.2. Dipoles

6.2.1. Design Considerations

The Proton Driver dipole is a conventional H-magnet design with Rogowsky profiled pole edges to help maintain field homogeneity at higher excitations. The lamination cross-section is shown in Figure 6.1 and a list of relevant parameters is presented in Table 6.1. The dipoles are excited so as to produce a magnetic field strength of the form

$$B(t) = B_0 - B_1\cos(\omega t) + 0.125B_1\sin(2\omega t) \tag{6.4}$$

where B_0 is the injection field, B_1 is the magnitude of the fundamental component and $\omega/2\pi = f = 15$ Hz. The second harmonic component is introduced to flatten the RF accelerating voltage, resulting in substantial RF system cost savings. Both the magnetic field ramp and its derivative are shown in Figure 6.3. Field homogeneity over the largest possible fraction of the physical aperture is obtained by shimming the pole pieces edges. The shim effectiveness can be estimated theoretically using formulas developed by K. Halbach [1]. Referring to Figure 6.4, assume the origin of the x-axis is situated exactly at the pole edge and that the pole continues to infinity for $x > 0$. At any fixed horizontal position x and, in particular at $x = 0$, the complex field is an even function of the vertical position y can be expanded in a

Table 6.1: Proton Driver Main Dipole Magnet Parameters

Max Stored Energy (5.1655 m)	0.336	MJ
Inductance (low field)	3.07	mH /m
Inductance (@ 1.5 T, with saturation)	2.88	mH /m
No of Turns/pole	2(parallel) $\times$ 12 = 24	
Transfer Constant (linear, $\mu = \infty$)	2.365×10^{-4}	T/A
Peak Dipole Field	1.5	Tesla
Peak Current (M17, including saturation)	6720	A
Steel Length	5.1655, 4.1924	m
Conductor Dimensions	37×37	mm^2
Conductor cooling tube dimensions	8 ID, 10 OD	mm
Conductor Packing Fraction	80% (approx)	
Physical Aperture	5×12.5	in^2
Good Field Aperture	5×9.0	in^2
Coil Area	0.105	m^2
Lamination Area	1.109	m^2
Lamination Thickness	0.014	in
Lamination Material	M17 Steel	
Core mass (5.1655 m magnet)	44,900	kg
Coil mass (5.1655 m magnet)	10,700	kg
Maximum Terminal Voltage (16 GeV, 5.1655 m magnet)	5	kV

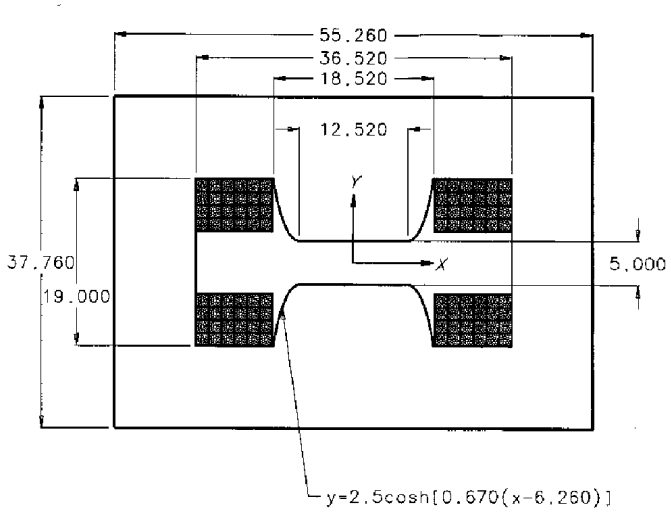

Figure 6.1: Proton Driver dipole cross-section.

Fourier series of the form

$$H_y + jH_x = \sum_{n=-\infty}^{\infty} C_n \exp \frac{n\pi jy}{g} \tag{6.5}$$

where g is the total vertical gap and the C_n are complex constant coefficients. Since the two-dimensional complex magnetic field in the aperture region must be an analytic function, (6.5) can be analytically continued over the entire aperture region

$$H_y + jH_x = \sum_{n=-\infty}^{\infty} C_n \exp \frac{n\pi z}{g} \tag{6.6}$$

where $z = x + jy$. The coefficients C_n must vanish for $n > 0$ since

$$|\exp \frac{\pi nx}{g}| \to \infty \quad x \to \infty \tag{6.7}$$

Thus,

$$H_y + jH_x = \sum_{n=-\infty}^{0} C_n \exp \frac{n\pi z}{g} \tag{6.8}$$

Note that $C_0 = H_{y0}$ represents the field deep into the aperture region. Let d be the the pole overhang, as shown in Figure 6.4. Without shims, the first few low order harmonics dominate the field deviation from uniformity. Considering only the first $(n = -1)$ harmonic, the field error at the edge of the good field region is

$$\frac{\Delta B}{B} = \frac{\Delta H_y}{H_{y0}} \simeq h_1 \exp \frac{-\pi d}{g} \tag{6.9}$$

where

$$h_n = \frac{1}{H_{y0}} \Re\{C_n\} \tag{6.10}$$

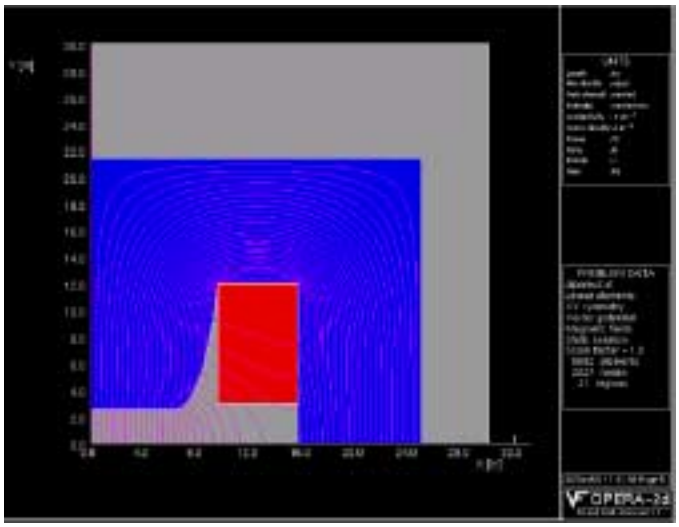

Figure 6.2: Proton Driver dipole flux lines.

A properly designed shim should suppress the first few spatial harmonics. Assume, for simplicity, that only the the first harmonic is suppressed. In that case, the second dominates and

$$\frac{\Delta B}{B} = \frac{\Delta H_y}{H_{y0}} \simeq h_2 \exp \frac{-2\pi d}{g} \tag{6.11}$$

In practice, one needs to consider more than one harmonic in order to accurately determine field homogeneity. Nevertheless, Halbach found that a simple two-parameter empirical relation of the form

$$\frac{\Delta B}{B} \simeq \lambda_1 \exp \frac{-\lambda_2 d}{g} \tag{6.12}$$

is generally adequate. The values of λ_1 and λ_2 are obtained by fitting results obtained numerically from two-dimensional calculations. In absence of shims, Halbach found that the overhang necessary to achieve a field homogeneity $\frac{\Delta B}{B}$ fits the relation

$$2d/g = -0.36 \log(\frac{\Delta B}{B}) - 0.9 \tag{6.13}$$

assuming that good field means $\frac{\Delta B}{B} < 1.0 \times 10^{-3}$, with $g = 5$ in, one gets

$$d \simeq 4.0 \text{ in} \tag{6.14}$$

Similarly, with shims, Halbach finds that the amount of necessary overhang fits the relation

$$2d/g = -0.14 \log(\frac{\Delta B}{B}) - 0.25 \tag{6.15}$$

that is, once again, with $\frac{\Delta B}{B} < 1.0 \times 10^{-3}$ and $g = 5$ in,

$$d \simeq 1.8 \text{ in} \tag{6.16}$$

Note that the empirical coefficients $\lambda_2 = 1/0.36 = 2.78$ and $\lambda_2 = 1/0.14 = 7.14$ are not too different from the values π and 2π predicted by the single dominant harmonic assumption.

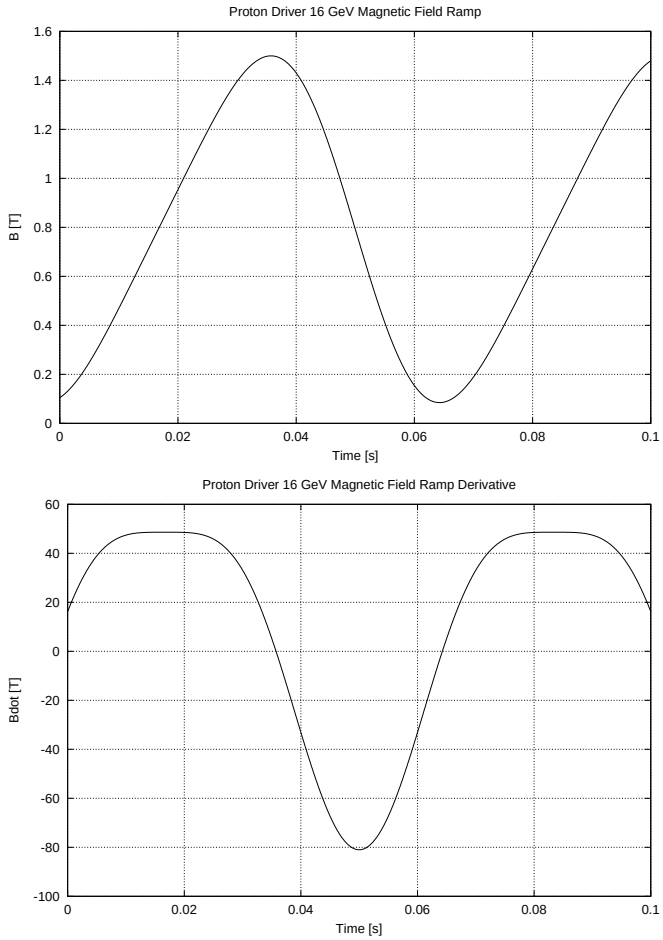

Figure 6.3: Magnetic field ramp and its derivative for 16 GeV operation ($B_0 = 0.7923$ T, $B_1 = 0.6876$ T). The RF accelerating voltage is proportional to the derivative of the magnetic field.

Halbach's formulae predictions are approximate and in principle, it should be possible to achieve better homogeneity with a complex shim. However, they provide a safe and conservative estimate. Figure 6.5 compares calculated low excitation field homogeneities for shimmed and unshimmed versions of the Proton Driver dipole magnet. The shim used in this example is a simple one-parameter rectangular shim.

The magnet cores are assembled from 0.014 in (29 gage) thick Si-Fe M17 laminations, of the type used in power transformers. For Si-Fe at 15 Hz, the skin depth $\delta \simeq 1$ mm = 0.040 in. In principle, one could use even thinner laminations to further reduce losses, but they become hard to handle.

Compared to low carbon steel used in slow ramping accelerators, Si-Fe has the advantage of reduced coercivity and conductivity; this helps reduce hysteresis and eddy current losses respectively. In principle, Si-Fe should be marginally more expensive to produce than low carbon steel; in practice, economies of scale and widespread availability due to applications

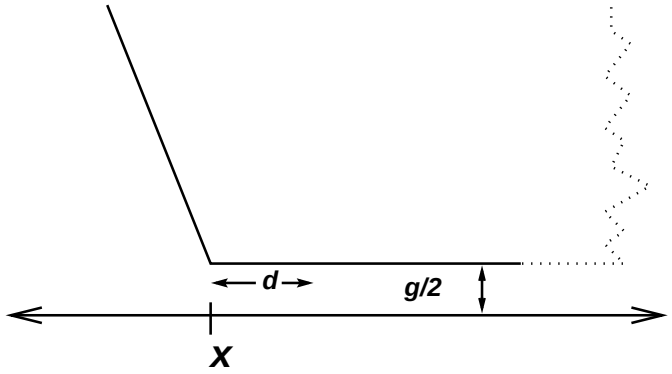

Figure 6.4: Idealized semi-infinite dipole magnet with pole overhang *d* and full gap is *g*. The horizontal origin is exactly at the outer edge of the pole and the field deep inside the aperture region is uniform.

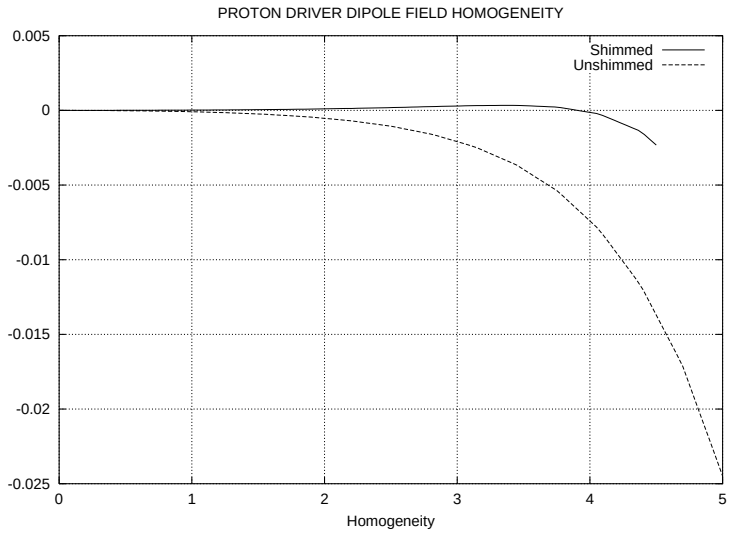

Figure 6.5: Proton Driver dipole field homogeneity at low excitation.

in the power industry more than compensate for this.

Virtually all manufacturer data on hysteresis and eddy current losses in Si-Fe corresponds to measurements performed at 50 or 60 Hz with a sinusoidal excitation. While simple scaling laws can be applied to estimate losses at 15 Hz, the Proton Driver magnet excitation also has a non-zero average component I_0, which corresponds to the injection energy. The presence of this component renders the hysteresis loops asymmetric. As a result, the standard scaling does not apply. To obtain a reliable estimate of the expected cyclic core losses, measurements were performed on a small core made out of M17 laminations. The results are summarized in Figure 6.6.

Macroscopic eddy current losses scale like the square of the frequency and the square of the peak field. In order to keep coil losses at reasonable levels, it was found necessary to use a special water cooled stranded conductor, as illustrated in Figure 6.7. This type of

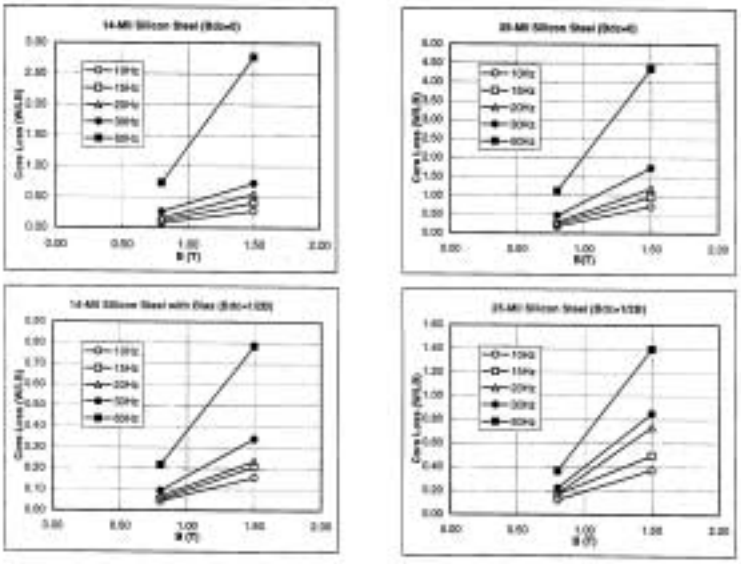

Figure 6.6: M17 Cyclic Steel loss measurements.

conductor is available commercially from at least two sources. The strands can be made out of either aluminum or copper. While for the former, inter-strand insulation is naturally provided by a layer of aluminum oxide, for the latter, a thin coat of "enamel" such as polyimide or polyamide-imide is necessary. Strands are are periodically transposed to provide uniform current distribution and lower losses. In general, the computation of conductor eddy current losses in conductors requires a self-consistent solution of Maxwell's equations (neglecting radiation). When the eddy currents induced by the quasi-statically computed fields are small with respect to the externally applied currents, they can be considered as a perturbation. This is often the case for eddy currents induced in the coils of slow ramping magnets; this is also the case for stranded conductors.

A quantity of interest is the resistance ratio R , defined as

$$R = \frac{R_{\mathrm{AC}}}{R_{\mathrm{DC}}} \tag{6.17}$$

where R_{AC} is the effective AC resistance, which is larger than the DC resistance R_{DC} for the same net current because of the different spatial current density distributions. Since the AC losses are proportional to R_{AC}, one can see that R is actually the ratio between the AC and the DC ohmic losses[1]. For the FNAL Booster (0.45 in $\times$ 0.45 in solid copper conductor with 0.25 in radius water cooling hole), numerical computations yield $R \simeq 2$. Assuming conductors of roughly the same type would lead to $R \simeq 8$ for the Proton Driver which is clearly not acceptable. We note in passing that there is practical limit for the size of water cooled conductor which is set by the surface to volume ratio of the cooling channel (which scales like $1/r$). While the volume of water flowing sets the water temperature rise, the

[1] In the present context, the term "AC losses" refers to the total time-averaged losses produced by a periodic current.

Figure 6.7: Stranded conductor.

surface area determines both the thermal and water flow resistance.

The eddy currents losses induced in a stranded conductor can be estimated in a straightforward manner. Consider, a circular strand of radius r immersed in a time-varying magnetic field $B(t)$ such as illustrated in Figure 6.8. Over the strand area, the magnetic field may be considered uniform. Using Maxwell's curl equation for the electric field, it is easily shown that the induced eddy current is

$$J_{\text{eddy}} \simeq \sigma x \dot{B} \tag{6.18}$$

provided that is small enough to be considered as a perturbation with respect to the total current. Integrating over the entire strand cross-section, one gets, for the instantaneous power loss per unit length (for one strand)

$$\begin{aligned} P_{\text{eddy}} &= \int \rho\sigma^2 x^2 (\dot{B})^2 \, dA & (6.19)\\ &= \int_0^{2\pi} \int_0^r \sigma r^3 (\dot{B})^2 \cos^2\theta \, dr d\theta & (6.20)\\ &= \frac{\pi}{4}\sigma r^4 (\dot{B})^2 & (6.21) \end{aligned}$$

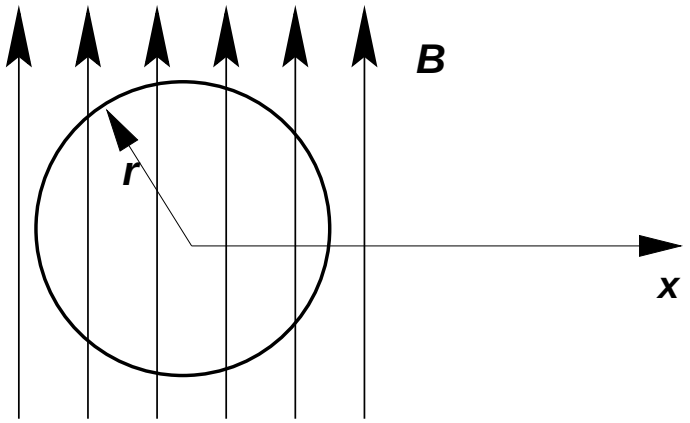

Figure 6.8: A circular strand immersed in a uniform, time varying magnetic field.

Over one excitation period, the rms average of $\dot{B}$ is

$$< \dot{B} >= \frac{3}{4}\omega B_1 \tag{6.22}$$

Thus,

$$P_{\text{eddy}} \simeq \frac{9\pi}{64}\sigma r^4 \omega^2 B_1^2 \tag{6.23}$$

and the resistance ratio R is

$$R = \frac{P_{\text{eddy}} + P_{\text{DC}}}{P_{\text{DC}}} \tag{6.24}$$

$$= 1 + \frac{9\pi}{64}\frac{r^4\omega^2 B_1^2}{\rho^2 J_{\text{DC}}^2} \tag{6.25}$$

For the Proton Driver dipole, $\omega = 30\pi$, $J_{\text{DC}} \simeq 1.92$ A/mm^2. Magnetostatic calculations show that the spatial rms average of the magnetic field over the coil cross-section is approximately 0.27 T when the gap field reaches 1.5 T. Using this value as representative of B_1 (although it is an overestimation) and assuming 2 mm Cu strands ($\rho = 1.7 \times 10^{-8}$ ohm-m), we get

$$R - 1 = \frac{9\pi}{64}\frac{(2\times 10^{-3})^4 (30\pi)^2 (0.27)^2}{(1.7\times 10^{-8})^2 (1.92\times 10^6)^2} \simeq 10^{-5} \tag{6.26}$$

a result which validates the assumption that eddy currents are a perturbation under these conditions.

Although the AC resistance of the stranded cable is expected to be only slightly larger than its DC resistance, it should be noted that because of the transposition, the stranded conductor is effectively longer than a solid conductor of identical total cross-section.

In order to minimize the overall inductance of the magnet and keep the voltage to ground below 5 kV, two pairs of top-bottom pancake coils are connected in parallel to provide the total magnet excitation.

Because of the large amount of magnetic energy stored in the magnets and its impact on the power supplies, the ratio of magnetic energy stored in the aperture region as a fraction of the total stored magnetic should be maximized. While profiled poles help maintain field homogeneity and linearity up to 1.5T, this comes at the cost of storing a substantial amount of energy in the pole fringing regions. No systematic attempt has been made to optimize the magnet in that regard. It is likely that efficiency could be improved somewhat by positioning conductors in the mid-plane; this has to be weighed against increased sensitivity of the field quality on coil positioning and eddy currents as well as the need for mechanically more complex saddle shaped coils.

6.3. Quadrupoles

6.3.1. Design Considerations

The Proton Driver Quadrupoles are four-fold symmetric magnets. Both the horizontal and the vertical focusing quadrupoles are identical. Large aperture iron-dominated quadrupoles become difficult to build when the pole tip field approaches 1.5 T. Note that the field is maximum not at the pole tip, but near the edges of the truncated hyperbolic pole profiles, and saturation occurs in these regions first. If the beam occupies a large fraction of the aperture, a four-fold symmetric quadrupole magnet has the advantage of suppressing all field harmonics except those of order 4n (8n-pole). Thus, the first allowed harmonic is the 12-pole. In contrast, for an asymmetric lamination with a wider horizontal aperture, the first allowed harmonic would be the 8-pole. When the field in the aperture (at least for the circular region inscribed inside the pole tips) is expanded as a power series in (r/r_0) – where r_0 is the pole tip radius – contributions from each term become rapidly less important with increasing order.

In order to allow the quadrupole and dipole strength to track each other dynamically, the quadrupoles are on the same current bus as the main bending dipoles. The number of turns and the dimensions of the quadrupole are selected to match as well as possible the saturation behavior of the dipoles. Figure 6.11 is a plot of the tracking function as a function of the excitation current. At 16 GeV, the deviation is on the order of 2.5%.

6.4. Sextupoles

6.4.1. Design Considerations

The Proton Driver sextupole magnets have, just like the quadrupoles, the symmetry of the dominant multipole in order to suppress lower order field harmonics. The horizontal and

Table 6.2: Proton Driver Quadrupole Magnet Parameters.

Aperture (Inscribed circle radius)	3.3541	in
Peak Gradient (16 GeV)	8.7494	Tesla/m
Peak Current (M17, including saturation)	6500	A
Steel Length	1.6824^2	m
Transfer Constant ($\mu = \infty$)	1.37865×10^{-3}	T/m/A
Stored Energy (1.6824 m)	0.052	MJ
Inductance	1.481	mH/m
No of Turns/pole	8	
Conductor Dimensions	37×37	mm^2
Conductor cooling tube dimensions	8 ID, 10 OD	mm
Conductor Packing Fraction	80%	
Lamination Area	1.095	m^2
Coil Area	0.0929	m^2
Lamination Thickness	0.014	in
Lamination Material	M17 Steel	
Core mass (1.6824 m)	14,500	kg
Coil mass (1.6824 m)	1,400	kg
Max Terminal Voltage (1.6824 m)	0.425	kV

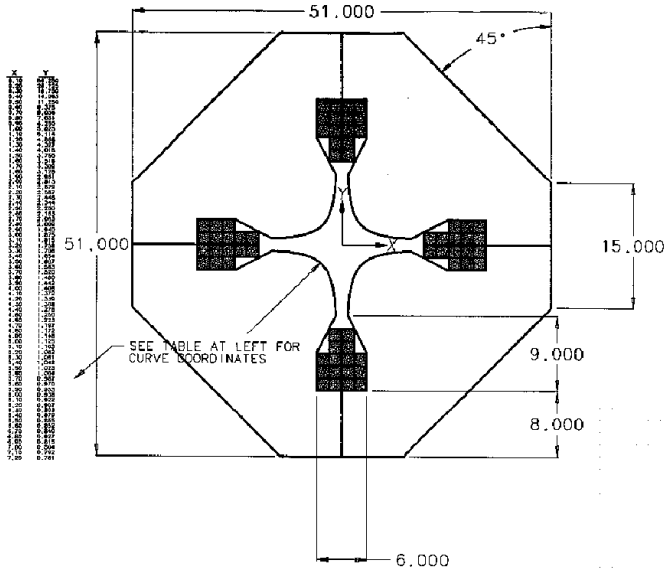

Figure 6.9: Proton Driver quadrupole cross-section.

vertical sextupoles cross-sections are identical; however, the backleg is dimensioned to accommodate the flux required by the strongest magnet. Sextupoles magnets are grouped in families; the families are powered by independent programmable supplies.

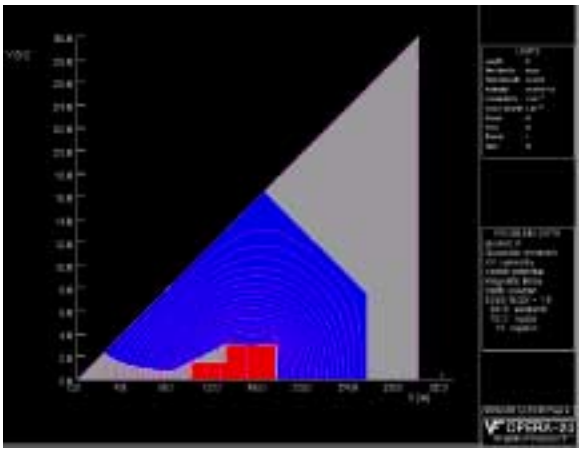

Figure 6.10: Proton Driver quadrupole flux lines.

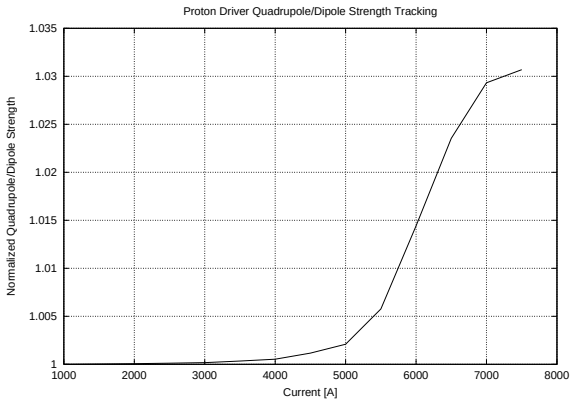

Figure 6.11: Normalized Quadrupole/Dipole strength tracking. At 16 GeV (common bus current of 6720 A), the deviation is approximately 2.5%. The residual tracking error is compensated by an active correction system.

6.5. Trim Magnets

Operational experience with ISIS has demonstrated that good orbit control during the entire acceleration cycle is one of the keys to loss minimization. This is not entirely surprising since small orbit changes typically result in small tune perturbations caused by change in overall orbit length and quadrupole feed-down in sextupoles.

6.5.1. Horizontal Dipole Correction

Due to space constraints in the lattice, all 48 main dipole bending magnets will include extra windings to integrate the function of *horizontal correctors*. Although the magnet described in this section does not include those windings, this should not pose fundamental difficulties. Nevertheless, it will be necessary to modify the lamination profile to accommodate the

Table 6.3: Proton Driver Sextupole Magnet Parameters.

Aperture (Inscribed circle radius)	3.818	in
Peak Sextupole (H,V)	35,47.5	T/m^2
Peak Current	2850	A
Steel Length	0.3	m
Max Stored Energy	2980	J
Inductance	2.448	mH/m
No of Turns/pole	4	
Transfer Constant ($\mu = \infty$)	0.016667	$T/m^2/A$
Conductor Dimensions	1.5×1.5	in^2
Lamination Thickness	0.014	in
Lamination Material	M17 Steel	
Lamination Area	0.5676	m^2
Coil Area	0.0696	m^2
Core Mass	1,340	kg
Coil Mass	190	kg

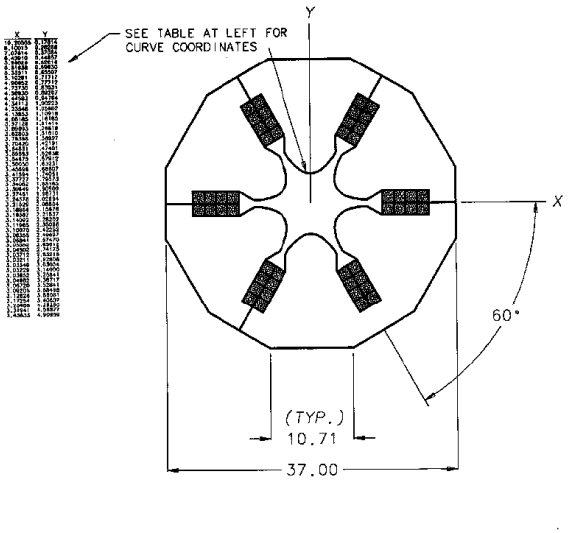

Figure 6.12: Proton driver sextupole cross-section.

correction windings. The electrical interconnections needed to suppress the large electromotive force induced by the main dipole flux are also a concern and will introduce additional complexity. The required horizontal correction is approximately 5 mrad, i.e. 3.8% of the bending angle of a dipole. Full range correction over the entire cycle requires a supplementary peak excitation of 5760 A-turn. The correction range could be reduced at high energy since it is envisioned that horizontal orbit corrections will be performed by physically moving quadrupoles.

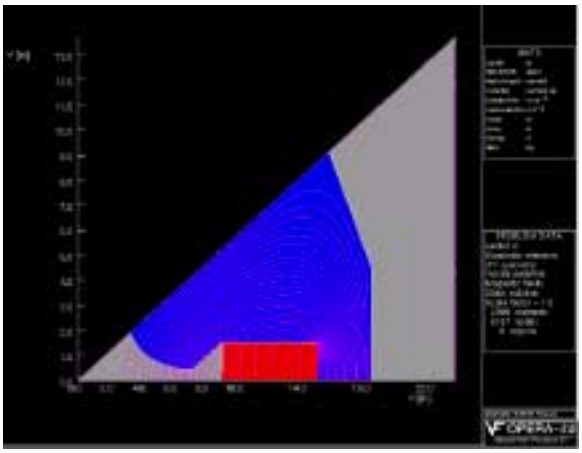

Figure 6.13: Proton driver sextupole flux lines.

6.5.2. Vertical Dipole Correction

The vertical correctors magnets are of a standard "pole-less" design, as shown in Figure 6.14. This has the advantage of providing good field quality even under moderate saturation levels. The two coils are excited so as to produce counter-circulating fluxes, resulting in uniform horizontal field within the interior region, as well as a considerable amount of flux in the exterior region. The inefficiency is usually of little concern for such small orbit correction magnets although time-varying external leakage flux may affect nearby instrumentation. The vertical trims are capable of full range correction (± 5 mrad) below 3 GeV. There are 8 trims per arc for a total of 24 in three arcs. Assuming another 12 in three straights, the total number of vertical trims is 36.

Table 6.4: Proton Driver Vertical Trim Parameters

No of Turns/pole	3×48	
Max Current (including saturation)	400	A
Max Field (including saturation)	0.25	T
Steel Length	0.25	m
Lamination Material	M17	
Lamination Thickness	0.014	in

6.6. Beam Pipe Induced Field Distortion

The presence of high frequency magnetic fields renders difficult, if not impractical, the utilization of a conventional beam chamber. The eddy currents induced in such a chamber lead to very high resistive losses and significant magnetic field distortion. These effects can be

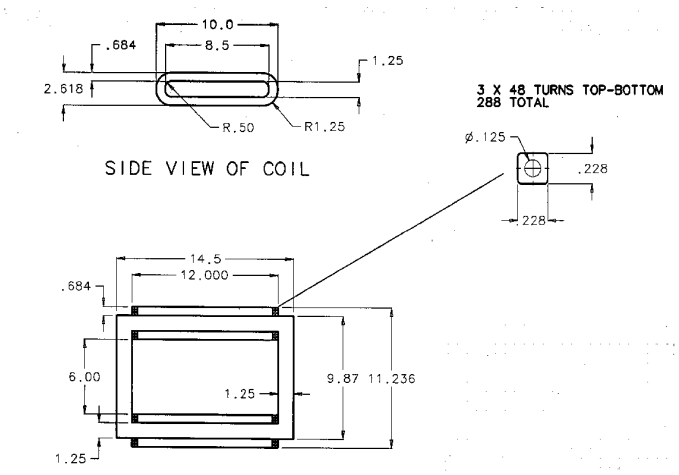

Figure 6.14: Vertical trim magnet cross-section.

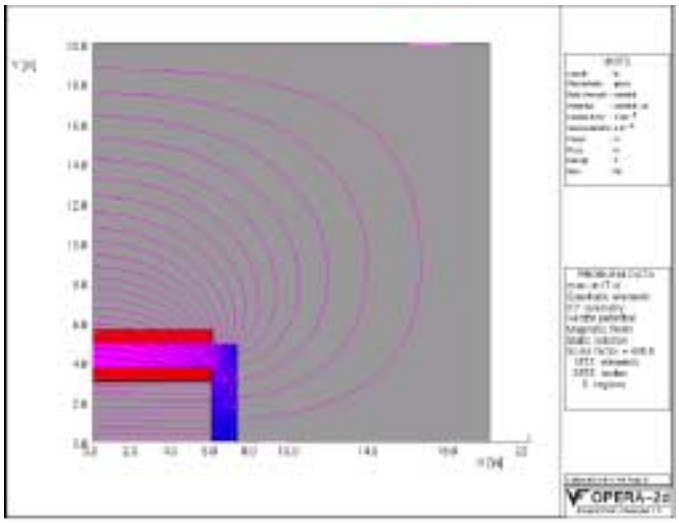

Figure 6.15: Vertical trim magnet flux lines.

reduced to a certain extent by making the vacuum chamber thinner; however, it has to be remain thick enough in order not to collapse. As described in Chapter 8, various alternatives to a conventional beam chamber have been considered. This report assumes that the beam chamber is eliminated by enclosing both the dipole and quadrupole magnets inside an external vacuum skins. While this approach results in a mechanically more complex magnet and in difficulties with out-gassing of magnet laminations and electrical coil insulation, it is a relatively well-established technology. One uncertainty, given the high beam intensity, is beam impedance minimization. It is envisioned that this will be accomplished by disposing closely spaced, thin metal strips on the pole face. To prevent eddy current flow, the strips are connected capacitively magnet-to-magnet.

While there are good reasons to be optimistic, it is possible that the strips may not provide sufficient impedance reduction. In that case, it may be necessary to resort to a “liner” similar in spirit to that proposed for the SSC or the LHC. Such a liner is basically a very thin

pipe with "random" holes to allow passage of the residual gas. The randomness of the hole pattern is necessary in order to avoid the introduction of new resonances.

Whenever a vacuum chamber or a liner is present, the time varying dipole field induces eddy currents within the chamber walls. As mentioned earlier, the magnitude of the induced current density is given by

$$J = \sigma E = \sigma x \dot{B} \tag{6.27}$$

These eddy currents in turn produce a magnetic field distortion which perturbs the field homogeneity. The distortion may be easily computed by subdividing the beam chamber into a number of filaments. Each of these filaments, assumed to be located between two infinitely permeable planes separated by a distance g, contribute a field

$$H_y + jH_x = \frac{I}{4g}\left(\tanh\frac{\pi(z-z_c^*)}{2g} + \coth\frac{\pi(z-z_c)}{2g}\right) \tag{6.28}$$

The total perturbation is the simply the sum of the filament contributions. The coefficients of the multipolar expansion of the field about the axis can be determined by differentiating this sum term by term. Using this approach, the multipoles induced during the proton driver acceleration cycle have been computed, assuming the parameters presented in Table 6.5. These parameters correspond approximately to the thinnest elliptical chamber capable of withstanding vaccuum pressure without collapsing. Note that the multipoles scale with the chamber thickness and resistivity; therefore, a liner could easily result in a magnetic field perturbation a few times smaller. If the perturbation is unacceptable, it can be passively compensated using a scheme which has been successfully implemented in the Brookhaven AGS Booster [3, 4]. Basically, a few turns of wire are fixed to the vacuum chamber. and the current in these wires is driven by a small coil wrapped around the pole. The circuit is closed by a small adjustable resistor.

Table 6.5: Vacuum chamber parameters used for Eddy current field distortion calculations. The distortion is proportional to both vacuum chamber thickness and wall conductivity.

conductivity	0.8×10^6	mho/m	(INCONEL)
wall thickness	1.27	mm	(50 mils)
major radius	11.43	cm	
minor radius	6.35	cm	
magnet gap	12.7	cm	

6.7. Research and Development

Fermilab has limited experience with rapid cycling magnets. The Booster magnets were fabricated more than thirty years ago; because of their relatively low field they were built

using technology similar to other conventional slow cycling magnets. In part because of an aggressive 1.5 T field, the Proton Driver magnets will need to use a special type of water-cooled stranded conductor. While this type of conductor is commercially available from the Japanese industry and has been used on a limited basis at KEK, the fact remains there is limited worldwide accumulated experience with such conductor. In particular, the following issues will require attention: (1) The minimum bending radius for cooled stranded conductor will be larger than for solid conductor of the same cross-section. Great care will be needed to engineer ends so as to minimize the longitudinal space allocated for the end region, especially in view of that fact that each magnet requires two set of coils connected in parallel in order to keep the inductance and the voltage to ground to acceptable levels. (2) The technology to make good electrical and mechanical joints in the conductor will need to be developed. (3) While it is believed that the stranded conductors described in this report would provide adequate cooling, this needs to be experimentally confirmed.

Another are of concern is high voltage operation. As described in this report, the dipole magnets have a maximum terminal voltage of 5 kV, which is somewhat aggressive. Voltage to ground insulation is a very important issue for magnet reliability and Fermilab has very limited experience with high voltage magnet technology. Although trouble spots are often concentrated in the vicinity of corners, they can be difficult to anticipate because they are very dependent on details of the magnet geometry that are difficult to include in computer models. The work involved in experimentally localizing troublesome high field regions and subsequently modifying magnet and coil geometries to even out electric stress distribution is potentially tricky and time-consuming.

Finally, high frequency operation will introduce small field distortions as well as a time lag between the excitation and the field and the presence of metallic strips or liner to reduce high frequency impedance will also perturb the field. These effects will need to be carefully measured for both the dipole and the quadrupole magnets. While the magnitudes of all these perturbations can be estimated, in view of the importance of minimizing particle losses, it would be extremely beneficial to conduct dynamic measurements of the transfer function (for dipole-quadrupole tracking) and field quality (including hysteresis effects) for both the dipole and quadrupole magnets. Much of the technology and expertise required could be developed by measuring an existing Booster magnet. Moreover, independently of the Proton Driver project, the information collected would be valuable to the existing program to help understand particle loss in the Booster.

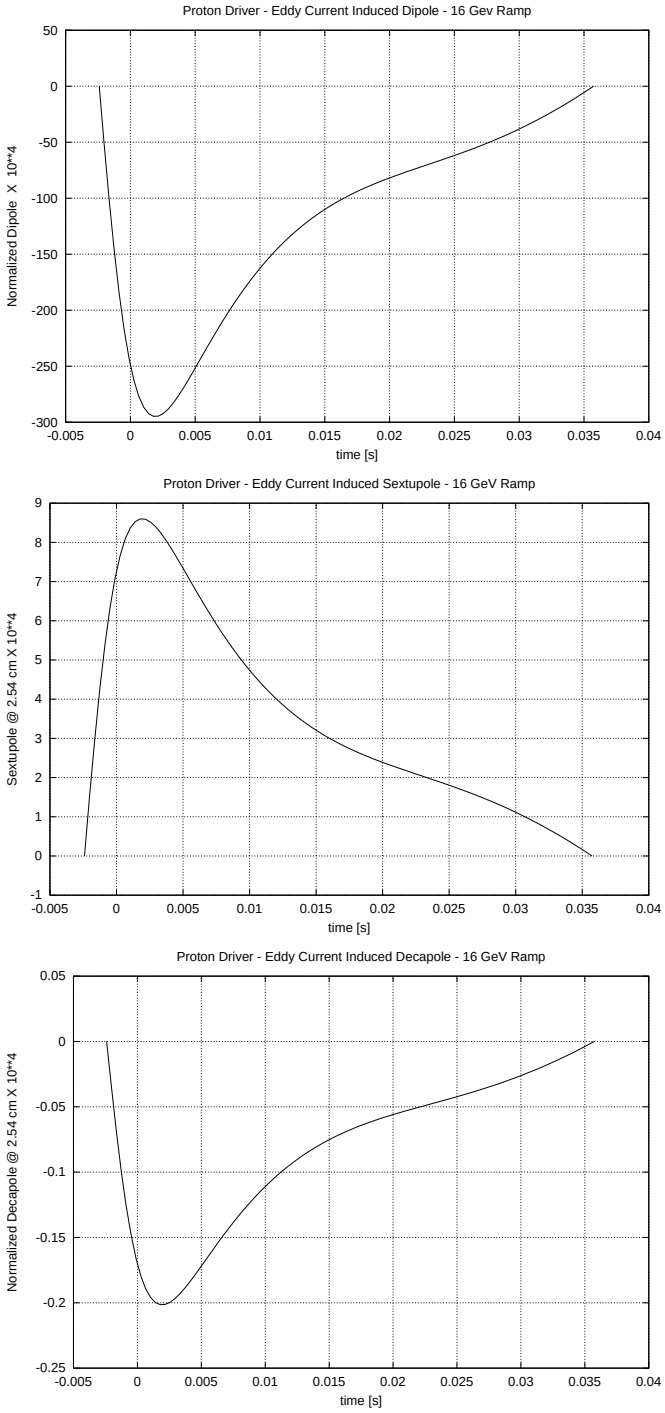

Figure 6.16: Normalized Dipole, Sextupole and Decapole variation during the acceleration cycle for 16 GeV (1.5 T peak dipole field.). The parameters in Table 6.5 have been assumed.

References

[1] A.W. Chao and M. Tigner Eds., *Handbook of Accelerator Physics and Engineering*, World Scientific, 1999.

[2] S.Y. Lee *A Multipole Expansion for the field of Vacuum Chamber Eddy Currents*, NIM A300, pp-151-158, 1991

[3] G.T. Danby, J.W. Jackson, *Description of New Vacum Chamber Correction Concept*, Proceedings of IEEE PAC 1989

[4] G.T. Danby, J.W. Jackson, *Vacuum Chamber Eddy Current Self-Correction for the AGS Booster Accelerator*, Particle Accelerators 27, pp 33-38 (1990)